nature medicine

Modeling colorectal cancer using CRISPR-Cas9–mediated engineering of human intestinal organoids

Mami Matano[1,4], Shoichi Date[1,2,4], Mariko Shimokawa[1,4], Ai Takano[1,4], Masayuki Fujii[1,3], Yuki Ohta[1], Toshiaki Watanabe[3], Takanori Kanai[1] & Toshiro Sato[1]

Human colorectal tumors bear recurrent mutations in genes encoding proteins operative in the WNT, MAPK, TGF-β, TP53 and PI3K pathways[1,2]. Although these pathways influence intestinal stem cell niche signaling[3–5], the extent to which mutations in these pathways contribute to human colorectal carcinogenesis remains unclear. Here we use the CRISPR-Cas9 genome-editing system[6,7] to introduce multiple such mutations into organoids derived from normal human intestinal epithelium. By modulating the culture conditions to mimic that of the intestinal niche, we selected isogenic organoids harboring mutations in the tumor suppressor genes *APC*, *SMAD4* and *TP53*, and in the oncogenes *KRAS* and/or *PIK3CA*. Organoids engineered to express all five mutations grew independently of niche factors *in vitro*, and they formed tumors after implantation under the kidney subcapsule in mice. Although they formed micrometastases containing dormant tumor-initiating cells after injection into the spleen of mice, they failed to colonize in the liver. In contrast, engineered organoids derived from chromosome-instable human adenomas formed macrometastatic colonies. These results suggest that 'driver' pathway mutations enable stem cell maintenance in the hostile tumor microenvironment, but that additional molecular lesions are required for invasive behavior.

Multiple mutations or 'hits' are thought to be required for the transformation of normal colon epithelium into invasive and metastatic colorectal cancer (CRC). The adenoma-carcinoma sequence model proposes a molecular basis for carcinogenesis[8]: loss of the *APC* gene (encoding adenomatous polyposis coli) first induces a premalignant precursor lesion (an adenoma), and subsequent mutations in genes including *KRAS* (encoding Kirsten rat sarcoma viral oncogene homolog), *SMAD4* (encoding SMAD family member 4) and *TP53* (encoding tumor protein p53) promote transformation to an invasive and metastatic phenotype[9]. Mutations in these genes are thought to drive colorectal carcinogenesis by deregulating driver pathways that modulate cellular proliferation, differentiation and apoptosis in order to confer selective growth advantages to mutated epithelium, including the WNT, RAS-MAPK, PI3K, TGF-β and TP53 pathways[6,7,10]. In rodent models, introducing combinations of two of these driver pathway mutations, such as *Apc* and *Kras*, Braf transforming gene (*Braf*) and *Trp53* or *Apc* and *Smad4*, induces intestinal adenocarcinoma[11–14]. In contrast, each human CRC often harbors 3–6 recurrent driver mutations[9], suggesting that higher numbers of driver mutations may be required for human colorectal carcinogenesis. Notably, the number of driver pathway alterations in human CRC is highly variable, with some CRCs carrying no pathway alterations or only one pathway alteration[1,2]. In these CRCs, somatic chromosomal aberrations or epigenetic lesions might instead alter driver pathway signaling. It is also possible that driver pathway alterations are dispensable in a subset of CRCs. To elucidate the role of driver pathway mutations in human CRC, a prospective analysis of the effects of site-directed mutations in the normal human colon epithelium is warranted, but this has long been hampered by the lack of a tractable culture system.

Recently, we developed an epithelial organoid culture system in which human intestinal stem cells (ISCs) indefinitely self-renew and form crypt-like organoid structures in Matrigel[15,16]. In this organoid culture system, human ISCs require a unique combination of Wnt, R-spondin, epidermal growth factor (EGF) and bone morphogenetic protein (BMP)/transforming growth factor (TGF)-β inhibitors, which mimic conditions in the ISC niche. In a physiological setting, these factors are locally provided by neighboring epithelial and mesenchymal cells[4,17] which restrict the self-renewal of ISCs to the narrow niche space at the crypt bottoms. In contrast, these niche factors are often dispensable for the growth of organoids derived from human CRC (as opposed to normal human epithelium)[15]. Because these niche factors influence most if not all of the pathways that are mutated in CRC, driver pathway mutations may modulate carcinogenesis by conferring selective growth advantages to ISCs[18]. As described here, to examine the influence of various driver pathway mutations on human colorectal carcinogenesis, we prospectively introduced multiple driver pathway mutations into human normal or adenoma-derived intestinal organoids.

To introduce defined genetic mutations in human intestinal epithelial cells, we used clustered regularly interspersed short palindromic repeat (CRISPR)–CRISPR-associated protein 9 (Cas9) genome editing[6,7,19] in human intestinal organoids (**Supplementary Fig. 1b**

[1]Department of Gastroenterology, Keio University School of Medicine, Tokyo, Japan. [2]Fujii Memorial Research Institute, Otsuka Pharmaceutical Co., Ltd., Shiga, Japan. [3]Department of Surgical Oncology, The University of Tokyo, Tokyo, Japan. [4]These authors contributed equally to this work. Correspondence should be addressed to T.S. (t.sato@a7.keio.jp).

Received 27 June 2014; accepted 14 January 2015; published online 23 February 2015; doi:10.1038/nm.3802

and **Supplementary Table 1**). First, we generated CRISPR-Cas9 sgRNAs targeting the *APC, SMAD4* and *TP53* tumor suppressor genes[20] (**Fig. 1**). Next, we dissociated human normal colonic organoids into single cells and electroporated the APC-targeting vectors into these cells; we then selected the cells in medium lacking Wnt and R-spondin. Under these culture conditions, single cells treated with control vector invariably ceased proliferation within 2–3 d, but the APC-targeted (A-) ISCs were able to form organoids (**Fig. 1b** and **Supplementary Fig. 2a**) in which mutations were detected by SURVEYOR (Transgenomic) assay. After clonal expansion of the single-cell derived A-organoids, the disruption of the targeted locus was confirmed by sequence analysis (**Fig. 1a**). As expected, western blotting showed the upregulation of β-catenin (**Supplementary Fig. 2b**). Next, we used similar methods to target *SMAD4* in dissociated normal organoids. As previously reported[15], normal intestinal organoids require noggin and a TGF-β receptor inhibitor (A83-01) for sustained growth. Thus, we selected SMAD4-targeted (S-) organoids in a medium lacking noggin and A83-01 but containing TGF-β or BMP4. Only S-organoids grew under these culture conditions (**Fig. 1d**). Subsequent cloning of single-cell–derived S-organoids showed indel mutations and loss of the SMAD4 protein (**Fig. 1c** and **Supplementary Fig. 2c,d**). Next, we targeted TP53 in dissociated normal organoids (**Fig. 1e**). Notably, TP53-targeted (T-) but not control organoids were readily recovered from cultures in medium containing nutlin-3, an inhibitor of MDM2 (ref. 21) (which degrades TP53) (**Fig. 1f**). Cloned T-organoids consistently showed indel mutations in the targeted locus (**Fig. 1e** and **Supplementary Fig. 2e**) and overexpressed a truncated stabilized form of TP53 (**Supplementary Fig. 2f**).

By using the genome-editing system established above, we next targeted *KRAS* that is downstream of EGF signaling by introducing the $KRAS^{G12V}$ hot spot mutation into A-organoids. To knock in the $KRAS^{G12V}$ mutation, we electroporated a sgRNA targeting a sequence adjacent to *KRAS* exon 2 together with a donor vector containing homologous arms but encoding the $KRAS^{G12V}$ mutation (**Fig. 1g**). Removal of EGF or addition of an EGF receptor (EGFR) inhibitor to

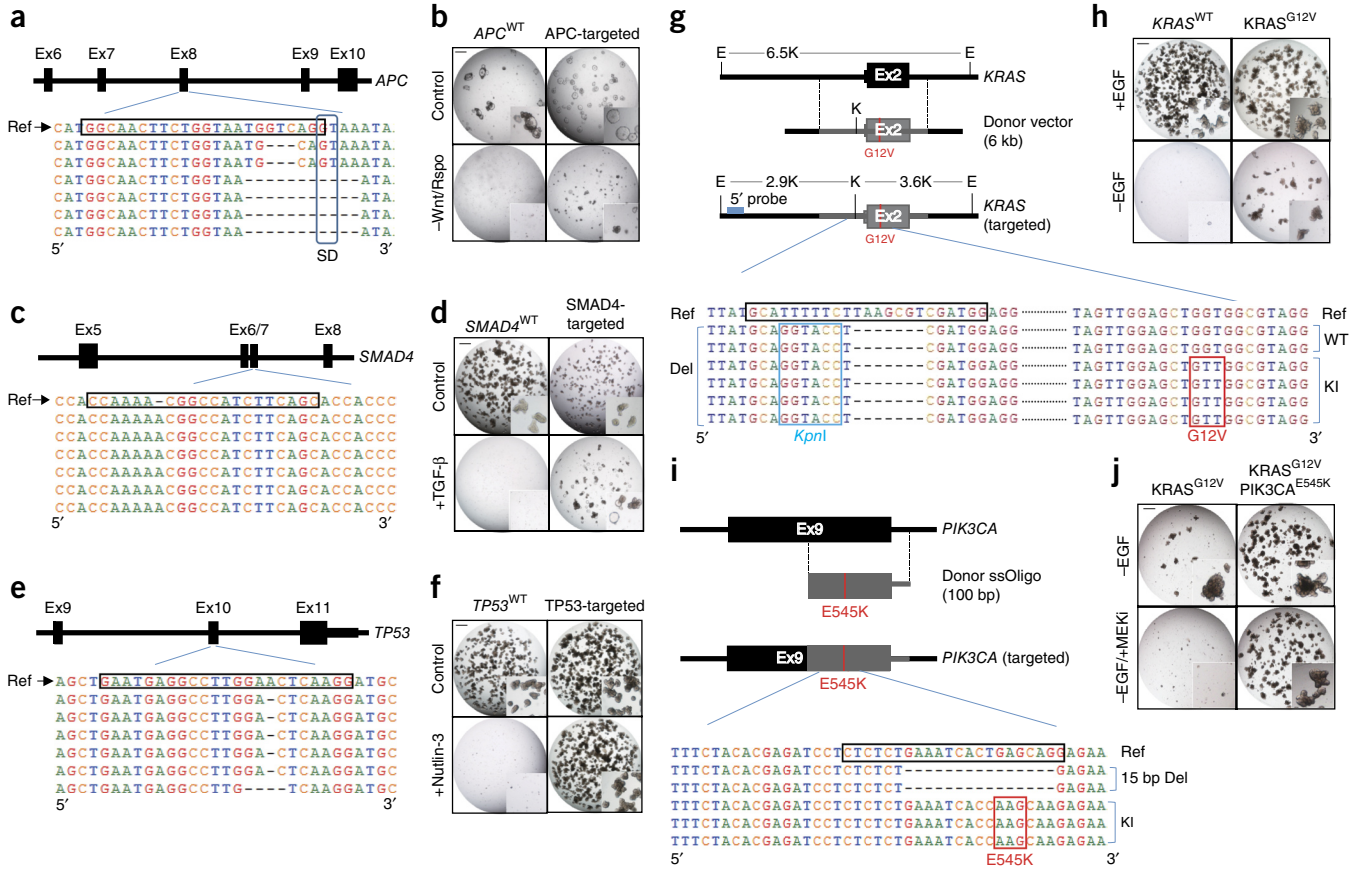

Figure 1 CRISPR-Cas9–mediated introduction of driver pathway mutations in human intestinal organoids. (**a**–**j**) Human intestinal organoids were dissociated into single cells and electroporated with sgRNAs targeting *APC*, *SMAD4* or *TP53*. (**a**,**c**,**e**) Sequences of targeted loci. Note that the splicing donor site is disrupted in one allele of *APC*. (**b**) Untargeted wild type (WT) or APC-targeted (A-) organoids were established and dissociated into single cells. The single cells were cultured in control medium (containing Wnt, EGF, noggin, R-spondin and A83-01) or medium lacking Wnt and R-spondin but containing EGF, noggin and A83-01. (**d**) Control or SMAD4-targeted (S-) organoids were cultured in control medium or medium lacking noggin and A83-01 but containing TGF-β. (**f**) Control or TP53-targeted (T-) organoids were cultured in control medium or medium containing the MDM inhibitor nutlin-3. (**g**) Strategy for targeting the human *KRAS* locus. The donor vector harbors the *Kpn*I site (light blue) and a G12V mutation (red) was co-electroporated to A-organoids. Sequences of six mutant alleles (Del) from targeted organoid clones are shown. Ref, reference sequence. Two of these clones show partial knock-in with wild-type codon 12 (WT). In the other four alleles, the homologous region is completely knocked in (KI). E: *Eco*RI, K: *Kpn*I. (**h**) Control $KRAS^{WT}$ A-organoids or $KRAS^{G12V}$ A-organoids were grown in control medium or medium lacking EGF. (**i**) Strategy for targeting the human *PIK3CA* locus. The donor ssDNA contains the E545K mutation (red). (**j**) $KRAS^{G12V}$ or $KRAS^{G12V}PIK3CA^{E545K}$ A-organoids were cultured in medium lacking EGF, or medium lacking EGF and containing a MEK inhibitor (MEKi). The results are representative of three different experiments performed in triplicate (**b**,**d**,**f**,**h**,**j**). Scale bars, 1 mm (**b**,**d**,**f**,**h**,**j**).

the culture medium blocked colony formation by untargeted ISCs, enabling the enrichment of organoids derived from $KRAS^{G12V}$-targeted ISCs (**Fig. 1h**). Homologous recombination in cloned $KRAS^{G12V}$ organoids was confirmed by Southern blotting and sequence analysis (**Fig. 1g** and **Supplementary Fig. 2g**). As expected, the efficiency of the mutation knock-in was lower than that observed after the introduction of indel mutations (**Supplementary Table 2**). Constitutive activation of KRAS was verified by ERK phosphorylation in $KRAS^{G12V}$ organoids in the absence of EGF (**Supplementary Fig. 2h**). Notably, the $KRAS^{G12V}$ mutation was not sufficient to fully substitute for EGFR signaling, as the removal of EGF decreased the growth efficiency of the $KRAS^{G12V}$ organoids (**Fig. 1h**). We next used CRISPR-Cas9 to activate another downstream signaling component of EGF—the PI3K-AKT pathway—in the $KRAS^{G12V}$organoids. A sgRNA targeting a locus adjacent to the mutational hot spot ($PIK3CA^{E545K}$) was electroporated into dissociated $KRAS^{G12V}$ organoids with a homologous donor oligonucleotide carrying the mutation (**Fig. 1i**). The $PIK3CA^{E545K}$ knock-in ($KRAS^{G12V}PI3KCA^{E545K}$) organoids selectively grew in the absence of EGF, in the same selection culture conditions used for $KRAS^{G12V}$ organoids (**Fig. 1j**). Addition of a mitogen/extracellular signal-regulated kinase (MEK) inhibitor, which blocks the downstream signaling of KRAS, to the culture medium–enriched $KRAS^{G12V}PI3KCA^{E545K}$ organoids from $KRAS^{G12V}$ (**Fig. 1j**). Recovered cloned organoids showed correct homologous recombination, which was confirmed by sequence analysis (**Fig. 1i**), as well as by phosphorylation of AKT (**Supplementary Fig. 2i**), an indicator of constitutive activation of PIK3CA. In contrast to the single $KRAS^{G12V}$ mutation, the $KRAS^{G12V}PIK3CA^{E545K}$ double mutations completely substituted for EGF signaling (**Fig. 1j**).

By using this genome editing and selection system for single-cells derived from organoids, we generated isogenic organoids carrying various combinations of driver gene mutations recapitulating the adenoma-carcinoma sequence (**Fig. 2a** and **Supplementary Fig. 1c**). We found that each culture condition was strictly specific to the corresponding pathway mutation, which enabled us to introduce various combinations of the pathway mutations in organoids without using conventional antibiotics-based selection (**Supplementary Fig. 1a**). After multiple cycles of cloning and CRISPR-Cas9–mediated targeting, engineered organoids progressively decreased the niche factor requirements (**Fig. 2b**). Accordingly, A-organoids were sensitive to treatment with EGFR, TGF-β, nutlin-3 or MEK inhibitors. With this antibiotic-free approach, we established AKSTP-organoids carrying

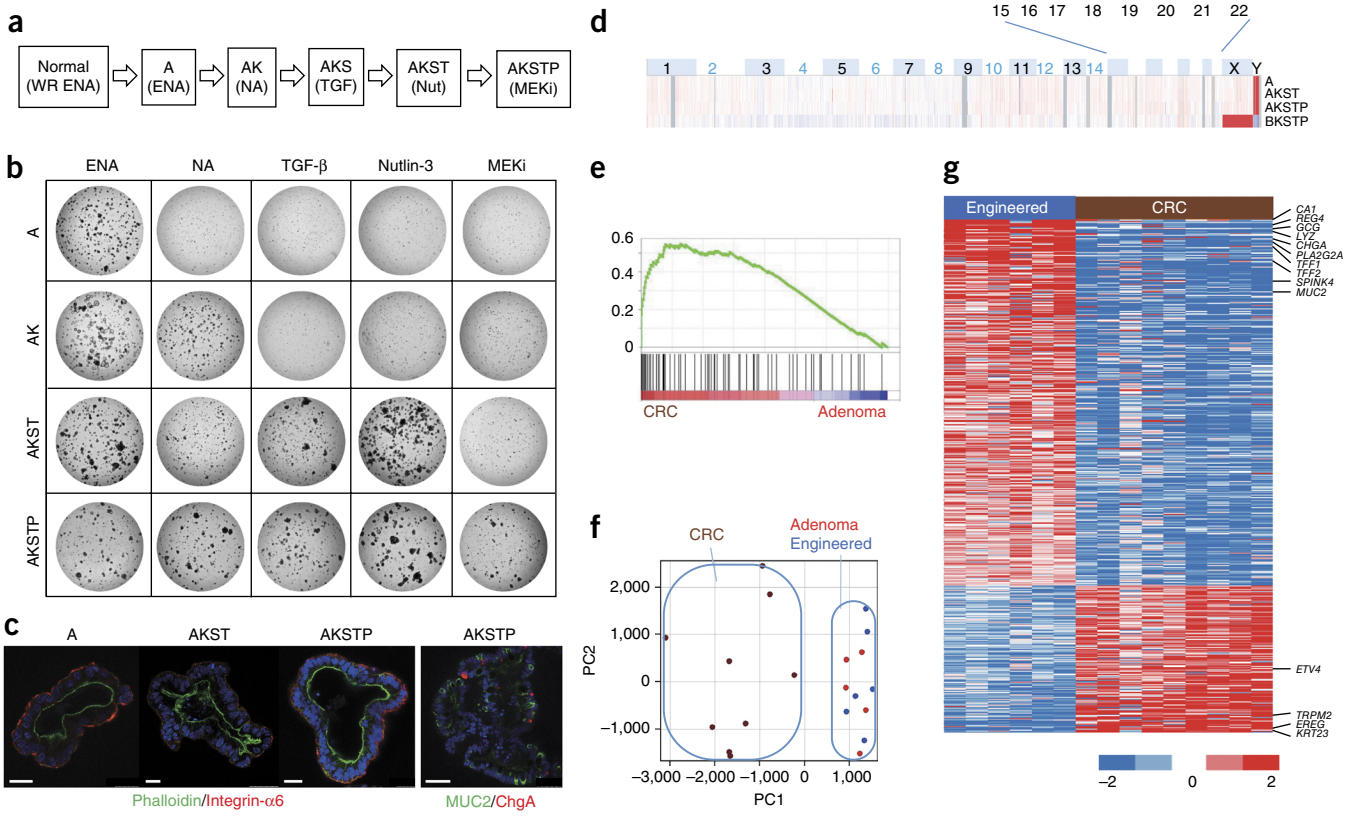

Figure 2 Sequential engineering of various combinations of driver mutations. (**a**) Strategy for establishing multiple driver mutations—to mimic the adenoma-carcinoma sequence—in organoids using CRISPR-Cas9. Engineered organoids were selected by the indicated niche factor–modulated culture conditions. W, Wnt-3A; R, R-spondin-1; E, EGF; N, noggin; A, A83-01; Nut, nutlin-3; TGF, TGF-β, MEKi, MEK inhibitor. Detected mutations (A, APC; K, $KRAS^{G12V}$; T, TP53; S, SMAD4; P, $PI3KCA^{E545K}$) are shown. Sequences are shown in **Supplementary Figure 8a**. (**b**) Driver gene mutations provide resistance to niche-modulated culture conditions. The results are representative of two different experiments performed in triplicate. (**c**) Immunostaining of engineered organoids. Left, F-actin stained by phalloidin (green) integrin-α6 (red). Right, MUC2, mucin 2 (green); ChgA, chromogranin A (red). Nuclear counterstain: Hoechst 33342 (blue). Scale bars, 50 μm. Results are representative of two different experiments. (**d**) Copy number analysis in engineered organoids. Blue and red indicate gain and loss of chromosome, respectively. See **Supplementary Figure 4** for detail of BKSTP. (**e**) Gene set enrichment analysis using CRC data sets (90 genes). Enrichment score = 1.721, False discovery rate = 0.003. (**f**) Principal component (PC) analysis of engineered organoids (blue), adenoma organoids (red) and CRC organoids (brown). (**g**) Heat maps showing the average $\log_2$-fold difference of the indicated genes between the engineered organoids and CRC organoids. See **Supplementary Figure 3** for heat maps including adenoma organoids.

five gene mutations (*APC, KRAS* (G12V), *SMAD4, TP53* and *PIK3CA* (E545K)), which grew completely independently of all niche factors described above (**Fig. 2b**). The engineered organoids were largely devoid of aneuploidy, copy number alterations (**Fig. 2d**), or CpG-island methylator phenotype (CIMP) (not shown), indicative of the maintenance of genetic stability during the course of organoid culture and gene manipulation. In addition to their nearly normal genetic status, whole-mount immunohistochemistry revealed intact apico-basal polarity and multiple features of well-differentiated colonic epithelium within the engineered organoids (**Fig. 2c**).

We next investigated the effect of driver pathway mutations in human intestinal epithelium on global gene expression patterns. Five lines of adenoma organoids and nine lines of CRC organoids were established and used for microarray analysis (**Supplementary Table 1**). To determine whether gene signatures of organoids represented their original tumor stage, we used adenoma and CRC gene expression data sets obtained from patients[22]. Gene set enrichment analysis (GSEA) indicated that the gene expression alteration during tumor progression was largely retained after organoid culture despite differences in micro-environments (**Fig. 2e**). Principal component analysis (PCA) among the three groups of organoids (CRC, adenoma and engineered) revealed similarity between the engineered and adenoma organoids (**Fig. 2f**). In the genes differentially expressed between engineered and CRC organoids, the engineered organoids were enriched for genes related to secretory differentiation (for example, *MUC2, SPINK4, TFF1* and *CHGA*), which are often lost in the course of colorectal carcinogenesis but retained in adenoma organoids[23] (**Fig. 2g** and **Supplementary Fig. 3**). By contrast, CRC-specific genes (for example, *EREG, TRPM2* and

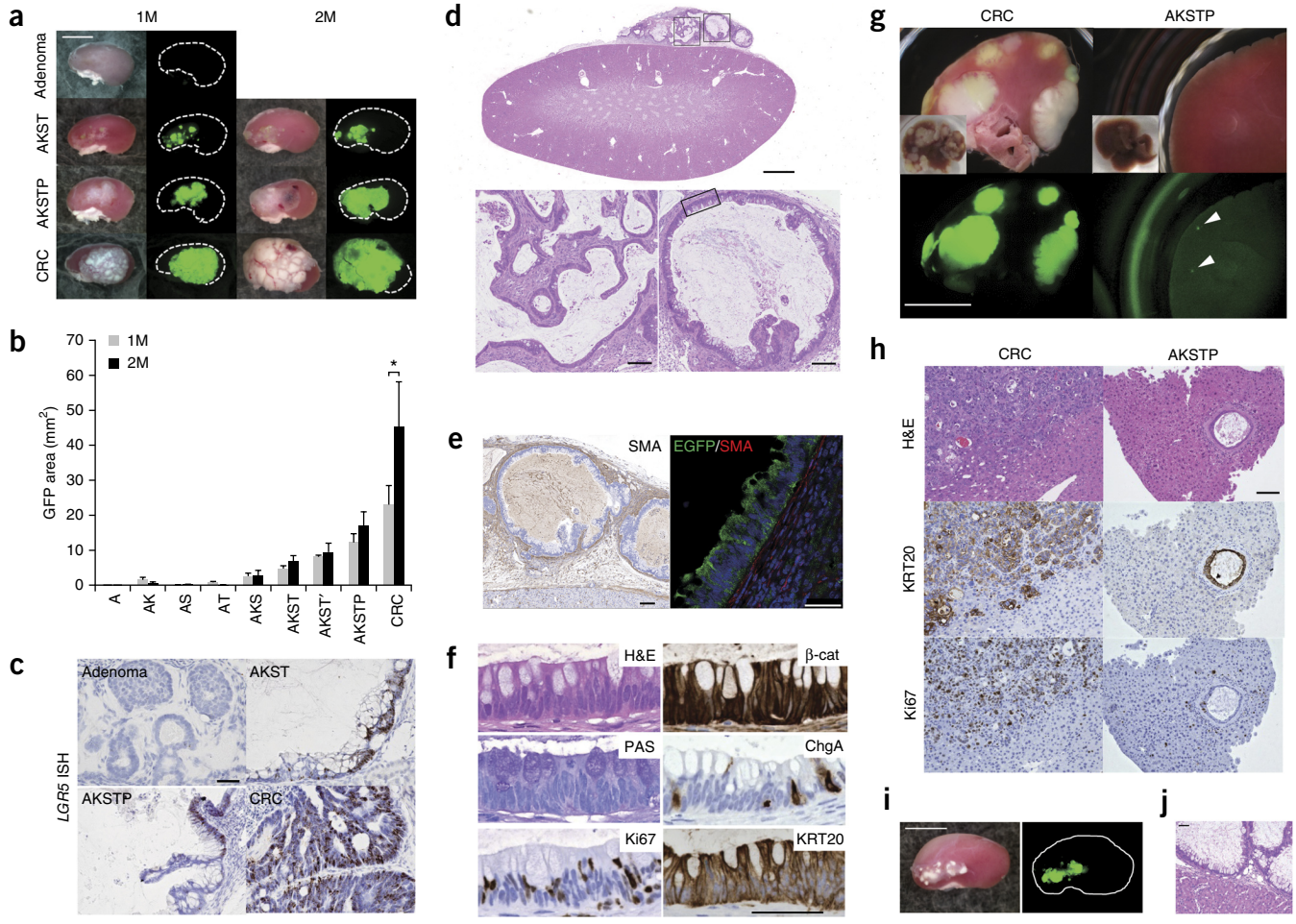

Figure 3 Engraftment of engineered, adenoma and CRC organoids in NOG mice. Indicated EGFP-labeled organoids were implanted under the kidney capsule of NOG mice. (**a**) Photographs of four representative tumors isolated 1 month (1M) or 2 months (2M) after the transplantation. (**b**) Average surface area of xenografts derived from organoids at 1 or 2 months after transplantation ($n = 4$ at each time point). The value of CRC is the average of six individual lines of CRC organoids ($n = 24$). Error bars indicate sem, $^*P < 0.05$. (**c**) *In situ* hybridization of *LGR5* mRNA (brown) in xenografts derived from organoids. (**d**) Representative HE staining of kidney subcapsule xenografts derived from AKSTP-organoids isolated 1 month after transplantation. Insets are magnified at bottom. The inset in the right panel indicates region shown in **f**. (**e**) Left, immunostaining of α-smooth muscle actin (SMA) in xenografts derived from AKSTP-organoids. Right, co-immunostaining of EGFP (green, human-derived organoids) and SMA (red). Nuclear counterstaining with Hoechst 33342 is shown in blue. (**f**) Immunohistochemistry of AKSTP tumors. β-cat, β-catenin; ChgA, chromogranin A; KRT20, cytokeratin 20. (**g**) Representative pictures of tumors that metastasized to the liver after injection into the spleen of NOG mice ($n = 4$ mice per genotype). Livers with metastatic lesions 2 months after the injection are shown. Top images show bright-field images of the hepatic lobule. Insets show bright-field images of the whole liver. Bottom images show an EGFP-fluorescent metastasized tumor in the hepatic lobule. Arrowheads indicate micrometastatic lesions. (**h**) H&E and immunostaining of metastasized organoids in the liver. (**i**) Tumor formation of organoids derived from AKSTP-micrometastatic lesions (1 month after transplantation). (**j**) Representative (of three images) H&E staining of tissue shown in **i**. Scale bars, 5 mm (**a**,**g**,**i**), 1 mm (**d,** top), 100 μm (**h**), 50 μm (**c**,**d** (bottom), **e**,**f**,**h**,**j**).

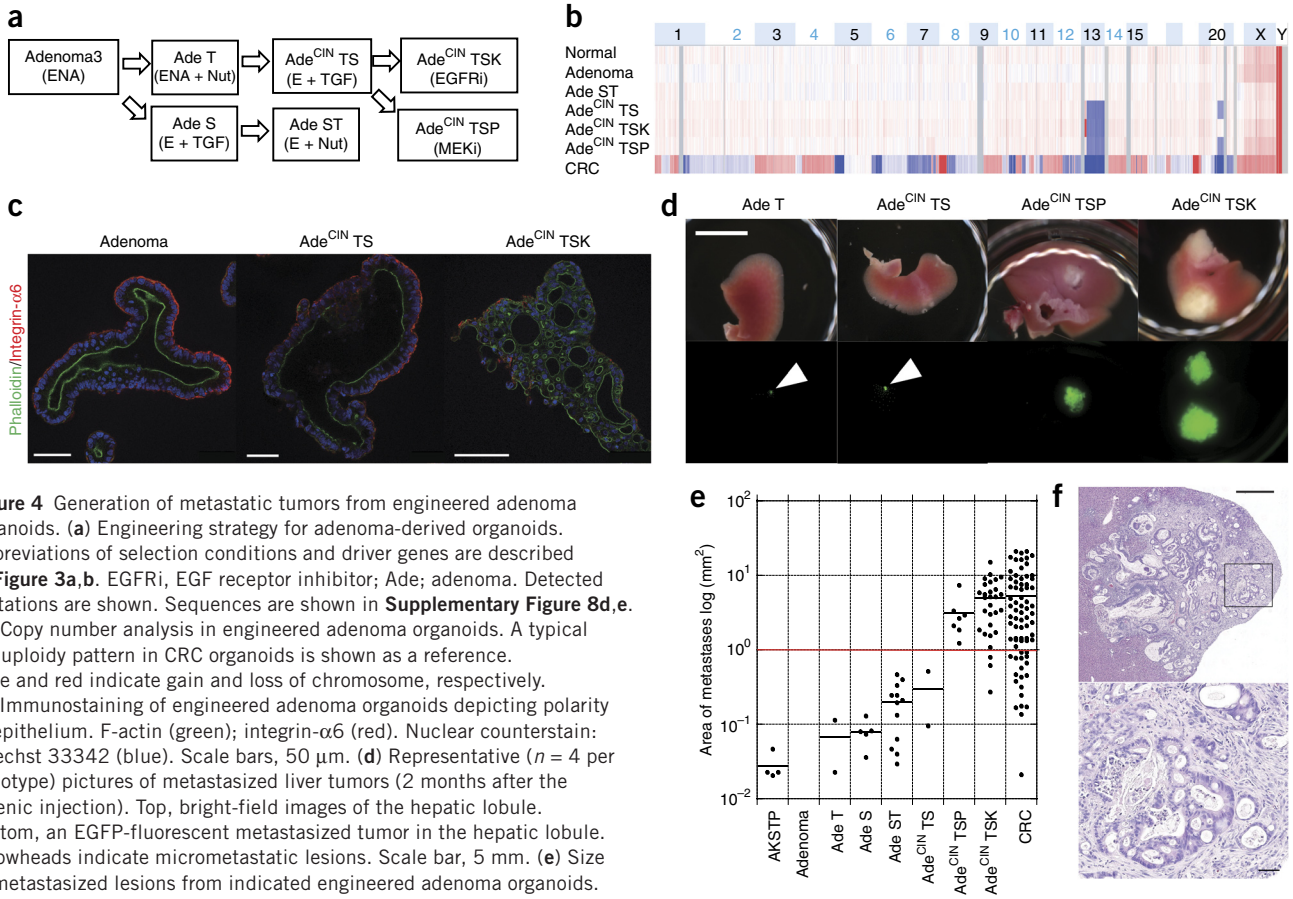

Figure 4 Generation of metastatic tumors from engineered adenoma organoids. (**a**) Engineering strategy for adenoma-derived organoids. Abbreviations of selection conditions and driver genes are described in **Figure 3a**,**b**. EGFRi, EGF receptor inhibitor; Ade; adenoma. Detected mutations are shown. Sequences are shown in **Supplementary Figure 8d**,**e**. (**b**) Copy number analysis in engineered adenoma organoids. A typical aneuploidy pattern in CRC organoids is shown as a reference. Blue and red indicate gain and loss of chromosome, respectively. (**c**) Immunostaining of engineered adenoma organoids depicting polarity of epithelium. F-actin (green); integrin-α6 (red). Nuclear counterstain: Hoechst 33342 (blue). Scale bars, 50 μm. (**d**) Representative ($n = 4$ per genotype) pictures of metastasized liver tumors (2 months after the splenic injection). Top, bright-field images of the hepatic lobule. Bottom, an EGFP-fluorescent metastasized tumor in the hepatic lobule. Arrowheads indicate micrometastatic lesions. Scale bar, 5 mm. (**e**) Size of metastasized lesions from indicated engineered adenoma organoids. For reference, metastatic lesions derived from AKSTP-engineered normal organoids or CRC organoids are indicated. Plots represent EGFP$^+$ area of metastasized lesions in liver. $n = 4$ mice per genotype. The number of plots indicate the total number of metastasized lesions in four mice. (**f**) Representative pictures of Ade^{CIN} TSK metastasized liver tumor. Top, low magnification. Scale bar, 500 μm. Bottom, high magnification of inset. Scale bar, 50 μm.

ETV4) were not expressed in the engineered organoids[1,24,25]. Although the biological impact of these gene expression changes remains unknown, our results suggest that driver pathway mutations and subsequent transcriptional changes are insufficient for the gene expression re-programming that occurs during the transition to CRC.

To determine the role of driver pathway mutations in human colonic tumorigenesis, we transplanted GFP-labeled organoids into kidney subcapsules of Nod-*scid*/*IL2Rγ*^{null} (NOG) mice[26,27] (**Fig. 3a**). The CRC organoids efficiently formed tumors that mimicked their parental histology, but the A-organoids or adenoma organoids showed no or minimal engraftment, suggesting that the kidney subcapsule is an unfavorable niche for benign epithelium (**Fig. 3a**,**b**). The engineered organoids acquired tumorigenic capacity in proportion to the number of mutations they harbored, as AKST- or AKSTP-organoids formed readily visible tumors (**Fig. 3a**,**b**). Isolated AKSTP tumors were re-propagated *in vitro* without niche factors (not shown). The tumor-derived AKSTP-organoids retained their original engineered mutations and could be re-engrafted under the kidney subcapsules of NOG mice (not shown). Consistent with their tumorigenic capacity, leucine-rich repeat–containing G protein–coupled receptor 5 (LGR5)$^+$ stem cells were detected in growing tumors from AKST- and AKSTP-organoids but not in remnants of engrafted adenoma organoids (**Fig. 3c**)[28]. We observed a similar tumorigenic capacity of engineered organoids derived from a second independent individual (AKST′ in **Fig. 3b** and **Supplementary Fig. 1**).

To assess off-target cleavage by CRISPR-Cas9, we examined potential off-target sites in AKSTP-organoids by exome sequencing (**Supplementary Table 3**). By using computer-based off-target prediction, we found that there were nine off-target sites carrying three base pair mismatches, of which six contained no mutations and the others were in the 3′UTR or intronic regions (**Supplementary Table 3**). We also analyzed 94 off-target sites with four mismatches, of which 70 were covered by exome sequencing without detecting mutations, and the others were in non-exonic regions (**Supplementary Table 3**). To further validate that the phenotypes we observed were due to specific mutations introduced by CRISPR-Cas9, we engineered organoids using lentiviruses[29] encoding shRNA to knock down *SMAD4* and *TP53* as well as transgenes encoding CTNNB1^{S33Y} (constitutively active form of β-catenin to activate WNT signaling), KRAS^{G12V} and PIK3CA^{E545K} (**Supplementary Fig. 4**). The resulting organoids, termed BKSTP-organoids, exhibited identical *in vitro* and *in vivo* phenotypes as those of AKSTP-organoids (**Supplementary Fig. 5**). These results suggest that driver gene mutations cooperatively substitute for niche signaling and confer selective growth advantages to ISCs in unfavorable microenvironments.

Histological analyses of AKST/AKSTP and BKSTP tumors revealed adenoma histology represented as well-ordered, highly differentiated epithelium encapsulated by mouse-derived stromal cells (**Fig. 3d–f** and **Supplementary Figs. 5** and **6**). Although AKSTP tumors had partial features of low-grade adenocarcinoma (**Fig. 3d**), their non-invasive

phenotype restricted their growth after 2 months. By contrast, most of the CRC organoids invaded adjacent tissue, resulting in constant enlargement of the tumor mass over 2 months (**Fig. 3b** and **Supplementary Fig. 6**). The functional difference between engineered and CRC organoids was even more evident when considering their metastatic ability. When injected into the mouse spleen, organoids derived from metastatic CRC successfully metastasized and colonized the liver, whereas AKSTP-organoids only formed micrometastatic lesions (<1 mm^2) (**Fig. 3g** and **Fig. 4e**). Histological analysis of AKSTP micrometastases depicted differentiated epithelium largely devoid of proliferation (**Fig. 3h**). Notably, cells from AKSTP micrometastases were capable of forming tumors after retransplantation into the kidney subcapsule, indicating that the micrometastatic lesions harbored dormant tumor-initiating cells (**Fig. 3i**,**j**). These results suggest that combinations of recurrent driver gene mutations contribute to niche-independent stem cell maintenance but not to metastatic progression.

In the adenoma-carcinoma sequence model, cytogenetic lesions are thought to drive tumor progression. However, control of chromosomal rearrangement of human primary cells is technically unfeasible. We engineered three lines of adenoma organoids (**Fig. 4a** and **Supplementary Figs. 1**,**7**–**9**) one of which showed a chromosomal instability (CIN) phenotype during the CRISPR-based engineering of TP53 and SMAD4 (hereafter referred to as Ade^{CIN} TS-organoids) (**Fig. 4a**,**b**). Similarly to parental adenoma organoids and AKSTP-organoids, Ade^{CIN} TS-organoids displayed highly polarized morphology and failed to macro-metastasize to the liver after injection into the spleen (**Fig. 4c**–**e**). However, after we used CRISPR-Cas9 to introduce a $KRAS^{G12V}$ mutation (Ade^{CIN} TSK-organoids) or lentivirus to introduce a $PIK3CA^{E545K}$ mutation (Ade^{CIN} TSP-organoids), these further-engineered Ade^{CIN} TSK/TSP-organoids showed cribriform-like dysplastic structures *in vitro* (**Fig. 4c**) and were capable of forming large metastatic tumors displaying histologic malignancy (**Fig. 4d**–**f**). A microarray analysis revealed no global gene expression changes during the metastatic transformation of the adenoma organoids (**Supplementary Fig. 7**). We confirmed no predicted off-target mutations in Ade^{CIN} TSK-organoids (**Supplementary Table 3**). Of note, CIN-negative adenoma remained non-metastatic after CRISPR-TSK or lentivirus-TSK engineering (**Supplementary Fig. 9**). Although the molecular mechanism of the metastatic progression remains unknown, these results suggest that genetic lesions other than driver pathway mutations are required for colon carcinogenesis.

The CRISPR-Cas9 system has been used to generate cancer cells from mouse primary cells or directly from *in vivo* tissue[30–33]. Here we established an efficient system to introduce multiple driver gene mutations into the human colonic epithelium by niche factor–modulated culture conditions, enabling clonal expansion of mutant stem cells without antibiotic selection. By using this niche-based selection system, we obtained quintuple pathway-mutant organoids, which grew independently of niche factors and formed tumors in hostile niche environments. Notably, most of CRC (>90%) as well as genetically engineered mouse CRC models possess fewer than five driver pathway alterations, suggesting that the non-mutated niche signaling in CRC could be complemented by adjacent non-epithelial mesenchymal or immune cells. Although driver pathway mutations increased the robustness of stem cells by hijacking niche signaling, driver pathway mutations *per se* were insufficient for malignant progression in this system. Interestingly, our results implicate chromosomal instability, in addition to driver pathway mutations, as required for invasive and metastatic transformation. Further studies will be required to elucidate the functional contribution of other molecular lesions, such as aneuploidy, copy number variations or epigenetic alterations in the malignant progression of human CRC in this system.

METHODS

Methods and any associated references are available in the online version of the paper.

Accession codes. Gene expression data have been deposited in the NCBI Gene Expression Omnibus with accession number GSE57965.

Note: Any Supplementary Information and Source Data files are available in the online version of the paper.

ACKNOWLEDGMENTS

This work was supported by grants from a research program of the Project for Development of Innovative Research on Cancer Therapeutics (P-Direct), by a Grant-in-Aid for Scientific Research on Innovative Areas 'Stem Cell Aging and Disease', and by Grants-in-Aid for Scientific Research, Ministry of Education, Culture, Sports, Science and Technology of Japan. T.S. received a Research Grant of the Japanese Society of Gastroenterology. T.S. would like to thank H. Clevers (Hubrecht Institute) for providing discussion and comments. We also thank M. Okumura for editorial assistance, Y. Tanada for animal care and the Collaborative Research Resources, School of Medicine, Keio University for technical assistance. The R-spondin–producing cell line was a kind gift from C. Kuo (Stanford University). F. Zhang (Massachusetts Institute of Technology) kindly provided the pX330 vector.

AUTHOR CONTRIBUTIONS

M.M., S.D., M.S., A.T., M.F. and Y.O. performed experiments. T.W. and T.K. provided biological specimens. T.S. conceived and designed the project. T.S. wrote the manuscript.

COMPETING FINANCIAL INTERESTS

The authors declare competing financial interests: details are available in the online version of the paper.

1. Seshagiri, S. *et al.* Recurrent R-spondin fusions in colon cancer. *Nature* **488**, 660–664 (2012).
2. Cancer Genome Atlas Network. Comprehensive molecular characterization of human colon and rectal cancer. *Nature* **487**, 330–337 (2012).
3. Sato, T. *et al.* Single Lgr5 stem cells build crypt-villus structures *in vitro* without a mesenchymal niche. *Nature* **459**, 262–265 (2009).
4. Sato, T. *et al.* Paneth cells constitute the niche for Lgr5 stem cells in intestinal crypts. *Nature* **469**, 415–418 (2011).
5. Sato, T. & Clevers, H. Growing self-organizing mini-guts from a single intestinal stem cell: mechanism and applications. *Science* **340**, 1190–1194 (2013).
6. Cong, L. *et al.* Multiplex genome engineering using CRISPR/Cas systems. *Science* **339**, 819–823 (2013).
7. Mali, P. *et al.* RNA-guided human genome engineering via Cas9. *Science* **339**, 823–826 (2013).
8. Vogelstein, B. *et al.* Genetic alterations during colorectal-tumor development. *N. Engl. J. Med.* **319**, 525–532 (1988).
9. Vogelstein, B. *et al.* Cancer genome landscapes. *Science* **339**, 1546–1558 (2013).
10. Fearon, E.R. Molecular genetics of colorectal cancer. *Annu. Rev. Pathol.* **6**, 479–507 (2011).
11. Rad, R. *et al.* A genetic progression model of Braf(V600E)-induced intestinal tumorigenesis reveals targets for therapeutic intervention. *Cancer Cell* **24**, 15–29 (2013).
12. Takaku, K. *et al.* Intestinal tumorigenesis in compound mutant mice of both *Dpc4* (*Smad4*) and *Apc* genes. *Cell* **92**, 645–656 (1998).
13. Onuma, K. *et al.* Genetic reconstitution of tumorigenesis in primary intestinal cells. *Proc. Natl. Acad. Sci. USA* **110**, 11127–11132 (2013).
14. Washington, M.K. *et al.* Pathology of rodent models of intestinal cancer: progress report and recommendations. *Gastroenterology* **144**, 705–717 (2013).
15. Sato, T. *et al.* Long-term expansion of epithelial organoids from human colon, adenoma, adenocarcinoma, and Barrett's epithelium. *Gastroenterology* **141**, 1762–1772 (2011).
16. Jung, P. *et al.* Isolation and *in vitro* expansion of human colonic stem cells. *Nat. Med.* **17**, 1225–1227 (2011).

17. Farin, H.F., Van Es, J.H. & Clevers, H. Redundant sources of Wnt regulate intestinal stem cells and promote formation of Paneth cells. *Gastroenterology* **143**, 1518–1529 (2012).
18. Vermeulen, L. *et al.* Defining stem cell dynamics in models of intestinal tumor initiation. *Science* **342**, 995–998 (2013).
19. Schwank, G. *et al.* Functional repair of CFTR by CRISPR/Cas9 in intestinal stem cell organoids of cystic fibrosis patients. *Cell Stem Cell* **13**, 653–658 (2013).
20. Ran, F.A. *et al.* Genome engineering using the CRISPR-Cas9 system. *Nat. Protoc.* **8**, 2281–2308 (2013).
21. Vassilev, L.T. *et al. In vivo* activation of the p53 pathway by small-molecule antagonists of MDM2. *Science* **303**, 844–848 (2004).
22. Carvalho, B. *et al.* Colorectal adenoma to carcinoma progression is accompanied by changes in gene expression associated with ageing, chromosomal instability, and fatty acid metabolism. *Cell. Oncol.(Dordr)* **35**, 53–63 (2012).
23. Noah, T.K. & Shroyer, N.F. Notch in the intestine: regulation of homeostasis and pathogenesis. *Annu. Rev. Physiol.* **75**, 263–288 (2013).
24. Baba, I. *et al.* Involvement of deregulated epiregulin expression in tumorigenesis *in vivo* through activated Ki-Ras signaling pathway in human colon cancer cells. *Cancer Res.* **60**, 6886–6889 (2000).
25. Chen, X., Halberg, R.B., Ehrhardt, W.M., Torrealba, J. & Dove, W.F. Clusterin as a biomarker in murine and human intestinal neoplasia. *Proc. Natl. Acad. Sci. USA* **100**, 9530–9535 (2003).
26. Ito, M. *et al.* NOD/SCID/gamma(c)(null) mouse: an excellent recipient mouse model for engraftment of human cells. *Blood* **100**, 3175–3182 (2002).
27. Kreso, A. & O'Brien, C.A. Colon cancer stem cells. *Curr. Protoc. Stem Cell Biol.* **7**, 3.1.1–3.1.12 (2008).
28. Merlos-Suárez, A. *et al.* The intestinal stem cell signature identifies colorectal cancer stem cells and predicts disease relapse. *Cell Stem Cell* **8**, 511–524 (2011).
29. Koo, B.K. *et al.* Controlled gene expression in primary Lgr5 organoid cultures. *Nat. Methods* **9**, 81–83 (2011).
30. Heckl, D. *et al.* Generation of mouse models of myeloid malignancy with combinatorial genetic lesions using CRISPR-Cas9 genome editing. *Nat. Biotechnol.* **32**, 941–946 (2014).
31. Xue, W. *et al.* CRISPR-mediated direct mutation of cancer genes in the mouse liver. *Nature* **514**, 380–384 (2014).
32. Platt, R.J. *et al.* CRISPR-Cas9 knockin mice for genome editing and cancer modeling. *Cell* **159**, 440–455 (2014).
33. Sánchez-Rivera, F.J. *et al.* Rapid modelling of cooperating genetic events in cancer through somatic genome editing. *Nature* **516**, 428–431 (2014).

ONLINE METHODS

Culture of human intestinal organoids. Surgically resected intestinal tissues or endoscopic biopsy samples were obtained from Tokyo University Hospital and Keio University Hospital. This study was approved by the Keio University Ethics Committee and Human Genome, Gene Analysis Research Ethics Committee, Graduate School of Medicine, the University of Tokyo. All samples were obtained from patients who provided informed consent before surgery or endoscopy. Adenoma, CRC and normal epithelia were isolated and cultured according to previously reported protocols[15]. The basal culture medium for human intestinal organoids was slightly modified from our original report as follows: Advanced Dulbecco's modified Eagle medium/F12 was supplemented with penicillin/streptomycin, 10 mM HEPES, 2 mM GlutaMAX, 1 × B27 (Life Technologies), 10 nM gastrin I (Sigma) and 1 mM N-acetylcysteine (Sigma). The following niche factors were used: 50 ng/ml mouse recombinant EGF, 100 ng/ml mouse recombinant noggin (Peprotech), 10% R-spondin-1 conditioned medium (kindly provided by C. Kuo, Stanford University)[34], 50% Wnt-3A conditioned medium[15], 500 nM A83-01 (Tocris) and 10 μM SB202190 (Sigma). To select mutant organoids, the following reagents were used: 10 ng/ml human recombinant TGF-β (R&D), 100 ng/ml human recombinant BMP4 (Peprotech), 1 μM EGFR inhibitor (EMD Millipore), 50 nM PD325901 (MEK inhibitor) (Sigma) or (±)-nutlin-3 (Cayman Chemical). For the organoid formation assay and before genome editing, organoids were dissociated into single cells with TrypLE Express (Life Technologies) and 1,000 cells were cultured in a 48-well plate under the above culture conditions for 10 d. To prevent anoikis, 10 μM Y-27632 was included in the culture medium for the first 2 d (ref. 3). The growth of organoids was estimated by area of intact organoids using bioimaging software (LuminaVision, Mitani Visual).

Genome engineering. Gene-specific sgRNA oligos were cloned into the px330 expression vector[20] (Addgene), which bicistronically expresses sgRNA and Cas9 nuclease. The sgRNA sequence was determined by the CRISPR Design Tool (http://crispr.mit.edu/) (**Supplementary Table 4**). After dissociating the organoids with TrypLE express, cells were electroporated with 10 μg of CRISPR-Cas9 plasmid (Neppagene). Cells were washed, embedded in Matrigel and cultured with optimal growth factors and Y-27632 (Sigma). For xenotransplantation assay, 7 μg of the *piggyBac* GFP-Puro expression vector and 3 μg of the PBase vector (SBI) were electroporated to fluorescently label the organoids. To knock-in an oncogenic mutation, 5 μg of sense or antisense donor ssOligo (manufactured by Life Technologies) or 5 μg of homologous recombination donor plasmid (constructed from pCR2.1 TOPO vector) was co-delivered with the sgRNA/Cas9 plasmid. Genomic DNA extracted from engineered organoids was used for the SURVEYOR assay (Mutation Detector kit, Transgenomics)[35] or Southern blotting analyses. For validation of targeted mutations, genomic DNA was isolated from cloned engineered organoids, followed by PCR amplification of targeted loci. PCR products were directly sequenced or cloned into a TOPO-TA cloning vector according to the manufacturer's instructions (Life Technologies). Plasmid DNA was isolated from eight bacterial clones and analyzed by Sanger sequencing (outsourced to Eurofins Genomics) to determine biallelic gene alterations. For whole-exome sequencing, genomic DNA was treated with an RNase Cocktail (Ambion) and outsourced to Hokkaido System Science.

Western blot analysis. The Matrigel surrounding the organoids was depolymerized by a Cell Recovery Solution (BD Biosciences). The released organoids were washed and pelleted. The pelleted organoids were lysed with Cell Lysis Buffer (CST) containing a protease/phosphatase inhibitor cocktail (Thermo Science) and phosphatase inhibitor cocktail set V (Calbiochem), and the organoids were further disrupted by sonication. Equal amount of SDS sample buffer was applied to the cell lysates. Protein was quantitated by the Bradford assay (Bio-Rad), and equal amounts of protein were loaded in each lane of a 4–20% SDS–PAGE. Standard western blot analyses were performed using the following primary antibodies: anti-β-catenin (610153, BD Biosciences, 1:1,000), anti-β-actin (A1978, Sigma, 1:1,000), anti-SMAD4 (sc-7966, Santa Cruz, 1:1,000), anti-TP53 (sc-98, Santa Cruz, 1:1,000), anti-ERK-1/2 (#9102, CST, 1:1,000), anti-phospho T^{202}/Y^{204} ERK-1/2 (#4370, CST, 1:1,000), anti-AKT-1/2/3 (#9272, CST, 1:1,000), anti-phospho T^{308} AKT (#4056, CST, 1:1,000) and anti-phospho S^{473}AKT (#9271, CST, 1:1,000). Signals were detected by HRP-conjugated secondary anti-rabbit antibody and visualized with the ECL Select LAS500 (GE Healthcare) and Image Quant LAS 500 (GE Healthcare).

Microarray and copy number analysis. Tumor organoids were expanded for gene expression analysis or copy number analysis. For gene expression microarray analysis, 500 ng of whole RNA was extracted from organoids using the RNeasy Mini Plus kit (Qiagen). Microarray hybridization was performed on the GeneChip Prime View Human Gene Expression Array (Affymetrix) according to the manufacturer's instructions. The data were analyzed with GeneSpring GX (Agilent). The microarray data are available in the GEO database (Accession number: GSE57965). GSEA was performed using open source software (v.2.0, Broad Institute, http://www.broadinstitute.org/gsea/index.jsp). A ranked gene list was created between adenoma and CRC organoids, and it was computed with a published pre-ranked list of upregulated genes in patient CRC specimens compared to those of adenoma[22]. The number of permutations was 1,000. For copy number analysis, the genomic DNA of organoids was extracted using the QIAamp DNA Blood Mini Kit (Qiagen) and analyzed by Cytoscan HD (Affymetrix). The copy number data were analyzed by Nexus copy number software (BioDiscovery).

Xenotransplantation of organoids. NOD.Cg-*Prkdc*^{scid}*Il2rg*^{tm1Sug}/Jic (NOG) mice (male, 7–12 weeks old) were obtained from the Central Institute for Experimental Animals (CIEA, Japan)[26] and housed under specific pathogen–free conditions. All procedures were approved by the Keio University School of Medicine Animal Care Committee. The GFP-expressing organoids were isolated from Matrigel using Cell Recovery Solution (BD Biosciences) and mechanically dissociated into small clusters of cells. The cell clusters (equivalent to 1×10^5 cells) were resuspended in cold Matrigel and injected under the kidney subcapsules or spleens of NOG mice. One or two months after transplantation, the kidney or liver was isolated, and the tumor size was measured by area of GFP fluorescence (Nikon Multi-zoom microscopy, LuminaVision software). A blinded investigator performed the measurement of the tumor size. The grafts were fixed for subsequent histological analysis. In some xenografts, tumor cells were isolated and subsequently cultured according to the methods described above. Each line of engineered organoids or CRC organoids was transplanted into 8 independent NOG mice. Four mice were used for analysis at each time point. The sample size was determined as the minimum size necessary to obtain a significant difference ($P = 0.05$) at a power of 80% when there was a 30% change in the tumor size. The time point of euthanasia was randomly assigned. As for inclusion/exclusion criteria for the xenograft experiments, we pre-determined to exclude data from mice euthanized because of sickness. We euthanized 2 out of 60 mice with implanted CRC organoids due to the tumor burden during the experimental period (2 months) and excluded these mice from the data analysis.

Immunohistochemistry and *in situ* hybridization. Whole-mount immunostaining was performed as previously described[3]. Isolated xenografts were immediately fixed with 4% paraformaldehyde. The standard protocol for sectioning paraffin-embedded tissues and H&E or Periodic acid-Schiff (PAS) staining was used. For immunohistochemistry, the following primary antibodies were used: anti-integrin-α6 (313601, Biolegend, 1:100), anti-Ki67 (RM-9106-S, Thermo Scientific, 1:300), anti-cytokeratin-20 (NCL-L-CK20, Leica, 1:50), anti-α-smooth muscle actin (MS-113-P, Thermo Scientific, 1:800), anti-EGFP (Ab6673, Abcam, 1:500), anti-Mucin2 (sc-15334, Santa Cruz, 1:100), anti-chromogranin A (sc-1488, Santa Cruz, 1:100) and anti-β-catenin (610153, BD Biosciences, 1:100). Secondary antibodies were polymer HRP conjugated anti-rabbit or mouse antibody (Nichirei Bioscience) for paraffin sections; Alexa Fluor 488 or 568 conjugated anti-rabbit, rat or goat antibody (Life Technologies) for whole-mount staining. Alexa Fluor 647–phalloidin (A22287, Life Technologies) was used for the visualization of F-actin. Nuclei were counterstained with hematoxylin (paraffin sections) or Hoechst 33342 (whole mount). For paraffin sections, staining was developed with DAB+ substrate chromogen (Dako). *In situ* hybridization for *LGR5* mRNA was performed with RNA Scope (Advanced Cell Diagnostics)

doi:10.1038/nm.3802

according to the manufacturer's instructions. The images of organoids were taken by either confocal microscopy (Leica SP8) or digital microscope (Keyence).

Lentiviral transduction. The VSV-G–pseudotyped third generation self-inactivating lentiviral vector was used for gene knockdown or overexpression. CTNNB1^{S33Y}, KRAS^{G12V} and PIK3CA^{E545K} were cloned into the pLenti CMV GFP Neo/Hygro/Puro/Zeo plasmid (Addgene). miR sequences targeting *SMAD4* and *TP53* were designed using The CRISPR Design Tool (http://crispr.mit.edu/) and inserted into the pcDNA6.2-GW/EmGFP-miR vector (BLOCK-iT Pol II mi RNAi kits, Life Technologies) (**Supplementary Table 4**). The miR vectors reduced the target gene expression by at least 80% in HEK293 cells. The viral vectors were transfected into HEK293FT cells with third-generation packaging plasmids (pLP1, pLP2 and pLP/VSVG; Invitrogen). The viral supernatant was passed through a 45-μm filter and centrifuged at 6,000*g* overnight. The titer of the viral supernatant was determined by qPCR and was typically higher than 10^7 titer units per ml. The organoids were dissociated into single cells and transduced with lentivirus as previously described[29]. Three days after the transduction, the infected organoids were selected with the appropriate antibiotics as follows: G418 (100 μg/ml), hygromycin (15 μg/ml), puromycin (2 μg/ml) and zeocin (200 μg/ml).

Statistical analysis. All results are expressed as mean ± sem and contain a minimum of $n = 4$ per group. We used unpaired Student's *t*-test or the analysis of the xenograft experiments. For gene expression microarray analysis, we used the Storey bootstrapping method. $P < 0.05$ was considered statistically significant. The experiments were not randomized.

34. Ootani, A. *et al.* Sustained *in vitro* intestinal epithelial culture within a Wnt-dependent stem cell niche. *Nat. Med.* **15**, 701–706 (2009).
35. Guschin, D.Y. *et al.* A rapid and general assay for monitoring endogenous gene modification. *Methods Mol. Biol.* **649**, 247–256 (2010).